ion aggregate structure and Eu^{3+} and UO_2^{2+} were expected to be uniformly dispersed throughout the polymer system so that the distances between Eu^{3+} and UO_2^{2+} were far beyond the energy transfer range.

These results further support the existence of ion aggregate structures in the PMM/MA system in which Eu^{3+} and UO_2^{2+} are located close together, facilitating the energy transfer between these ions.

The above conclusions attributing the loss of Eu^{3+} fluorescence activity at higher UO_2^{2+} concentration to UO_2^{2+} self-quenching can only be confirmed by a simultaneous study of the concentration dependence of both emissions and by measuring decay and build-up times of both. These experiments are now in progress and will be the subject of a future report.

Acknowledgment. This work was supported by a generous grant from the National Science Foundation under Polymer Programs Grant DMR-09764. We are grateful to Dr. S. Nakajima for X-ray powder diffraction analysis.

References and Notes

(1) Förster, Th. *Discuss. Faraday Soc.* **1959**, *27*, 7.
(2) Sinha, S. P. "Europium"; Springer-Verlag: New York, 1967; p 123.
(3) De Shager, L. G.; Cabeza, A. Y. *Proc. IEEE* **1964**, *52*, 1355.
(4) Kropp, J. L. *J. Chem. Phys.* **1967**, *46*, 843.
(5) Eisenberg, A. *Polym. Prepr., Am. Chem. Soc., Div. Polym. Chem.* **1979**, *20* (1), 286.
(6) Eisenberg, A.; King, M. "Ion-Containing Polymers"; Academic Press: New York, 1977; p 23.
(7) Banks, E.; Okamoto, Y.; Ueba, Y. *J. Appl. Polym. Sci.* **1980**, *25*, 359.
(8) Okamoto, Y.; Ueba, Y.; Dzhanibekov, N. F.; Banks, E. *Macromolecules* **1981**, *14*, 17.
(9) Witt, J. R.; Orstott, E. J. *J. Inorg. Nucl. Chem.* **1962**, *24*, 637.
(10) Taha, I. A.; Morawetz, H. *J. Am. Chem. Soc.* **1971**, *93*, 829.
(11) Barclay, G. A.; Sabine, T. M.; Taylor, J. C. *Acta Crystallogr.* **1965**, *19*, 205.
(12) Ohwada, K. *Spectrochim. Acta, Part A* **1968**, *24*, 595.
(13) Van Uitert, L. G. *J. Electrochem. Soc.* **1960**, *107*, 803.

Effect of Filament Flexibility on the Dynamic Light-Scattering Spectrum with Special Reference to fd Virus and Muscle Thin Filaments†

Tadakazu Maeda and Satoru Fujime*

Mitsubishi-Kasei Institute of Life Sciences, Machida, Tokyo 194, Japan.
Received January 6, 1981

ABSTRACT: The field correlation function, $g^{(1)}(\tau)$, of light scattered from very long, semiflexible filaments in dilute solution was simulated for various values of filament length (L), flexibility (γL), friction constant (ζ), temperature (T), and length of the scattering vector (K). For a given γL, $g^{(1)}(\tau)$'s for different temperatures scaled with T/η (η is solvent viscosity). In the stiff limit ($\gamma L \ll 1$), profiles of the present $g^{(1)}(\tau)$'s closely resembled those based on a rigorous formula for a rigid rod. In the semiflexible range ($0 \ll \gamma L \leq 0.5$), the profiles of $g^{(1)}(\tau)$'s strongly depended on γL at large K, indicating that if γL changes with temperature, $g^{(1)}(\tau)$'s do not scale with T/η at large K. The model was applied to the analysis of experimental data available in the literature and it was suggested that both fd virus and the muscle thin filament are not rigid but have γL values of the order of 0.1.

Introduction

Considerable effort has been expended in recent years in extracting the contributions of internal motions of large flexible macromolecules from the intensity autocorrelation functions of polarized Rayleigh scattered light. Pecora[1,2] was the first to give theoretical expressions for the field correlation function of light scattered from flexible-coil macromolecular chains as a sum of exponential terms with time constants corresponding to the lifetimes of the internal fluctuation normal modes. Fujime[3] and Fujime and Maruyama[4] gave formulas for the intensity fluctuation spectrum of light scattered from semiflexible filaments also as a sum of exponentials.

In earlier days of dynamic light-scattering studies, one used spectrum analyzers. More recently, however, one uses digital correlators. Since the power spectrum and the time correlation function are connected with each other by the Fourier transform, both techniques should provide the same information. However, the real situation is very different for these two techniques. Consider a model situation composed of four components:

$$g^{(1)}(\tau) = \sum_n P_n \exp(-\tau/\tau_n) \qquad \text{with} \qquad \sum_n P_n = 1$$

The so-called average decay rate $\bar{\Gamma}$ of $g^{(1)}(\tau)$ is given by $\bar{\Gamma} = \sum_n P_n/\tau_n$. Even if $P_1 > P_2 > P_3 \gg P_4$ and $\tau_1 > \tau_2 > \tau_3 \gg \tau_4$, the ratio P_4/τ_4 is not necessarily small compared with P_1/τ_1. Roughly speaking, the short-time behavior of correlation functions is sensitively affected by components having short time constants. On the other hand, the power spectrum corresponding to the above $g^{(1)}(\tau)$, in the heterodyne case for simplicity of discussion, has the form

$$S(\omega) = (1/\pi)\sum_n \{(1/\tau_n)P_n/[\omega^2 + (1/\tau_n)^2]\}$$

In the above situation of P_n and τ_n, the fourth Lorentzian in $S(\omega)$ will hardly be detected because $\pi S(0) = \sum_n P_n\tau_n$ and $\pi S(\omega_h)\omega_h^2 = \bar{\Gamma}$, where $\omega_h \gg 1/\tau_4$. Of course, $P_1\tau_1 > P_2\tau_2 > P_3\tau_3 \gg P_4\tau_4$ and only at frequencies $\omega \gtrsim \omega_h$, where $S(\omega)$ will be close to or below the noise level, will all components contribute to the power spectrum in the same way as to the correlation function. The power spectrum is insensitive to components having short time constants. From an experimental point of view, *we have to take into account many more components in the correlation technique than in the spectral technique.*

† A part of this work was presented at the NATO ASI on scattering techniques, Wellesley College, Mass., August 1980.

0024-9297/81/2214-0809$01.25/0

A three-exponential analysis in the correlation technique (or three-Lorentzian analysis in the spectral technique) is probably the best procedure possible, and any multiexponential (or multi-Lorentzian) analysis will not work well. However, we have to take into account a tremendous number of exponential terms in order to measure lifetimes of internal normal modes of *very* large macromolecules. In such a case, it seems to be more practical to directly compare computed correlation functions (or power spectra) based on a suitable model with experimental ones. de Gennes[5,6] was the first to give theoretical expressions of the field correlation function, without exponential expansion, for flexible-coil chains. Progress along this line in light scattering has been made in the cases of polystyrene in organic solvents[7,8] and DNA in saline solution.[9,10] This method is sometimes useful even in two-exponential cases.[11,12]

In this paper, we compute field correlation functions of light scattered from semiflexible, long filaments in order to see the effect of the filament flexibility on the dynamic light-scattering spectrum. Applications of the present result will be made to the analysis of experimental data of long virus particles and of muscle thin filaments.

Model

We first briefly review our model on the field correlation function, $g^{(1)}(\tau)$, for a semiflexible wormlike filament.[4]

The conformation of a macromolecular chain is expressed by a continuous, differentiable space curve, $\vec{r} = \vec{r}(s,t)$, where s is the coordinate of a line element ds measured along the chain having length L ($-L/2 \leq s \leq L/2$). The elastic potential energy of the chain is assumed to be given by

$$V = \tfrac{1}{2}\int_{-L/2}^{L/2}\{\epsilon(\partial^2\vec{r}/\partial s^2)^2 + \kappa(\partial\vec{r}/\partial s)^2\}\,ds \qquad (1)$$

where ϵ and κ are elastic constants of bending and stretching of the chain, respectively. Strictly speaking, this assumption contains some inconsistencies in the stiff limit.[13] But it is adopted again to make the equation of motion for the chain mathematically tractable. A differential equation of motion of the chain in solution can be derived from eq 1 with Hamilton's principle of least action[14] as

$$\rho(\partial^2\vec{r}/\partial t^2) + \zeta(\partial\vec{r}/\partial t) + \epsilon(\partial^4\vec{r}/\partial s^4) - \kappa(\partial^2\vec{r}/\partial s^2) = \vec{A}(s,t) \qquad (2)$$

where ρ is the linear mass density of the filament, ζ is the friction constant per unit length of the filament, and $\vec{A}(s,t)$ is the fluctuating Brownian force acting on the filament. The elastic constants have been given in terms of γ (inverse of the statistical length) as[14]

$$\epsilon = 3k_BT/4\gamma \quad \text{and} \quad \kappa = 3k_BTL/\langle R^2\rangle \qquad (3)$$

where

$$\langle R^2\rangle = [e^{-2\gamma L} - 1 + 2\gamma L]/2\gamma^2 \qquad (4)$$

By mode expansion

$$\vec{r}(s,t) = \sum_n \vec{q}(n,t)Q(n,s) \qquad (5a)$$

and

$$\vec{A}(s,t) = \sum_n \vec{B}(n,t)Q(n,s) \qquad (5b)$$

we have from eq 2

$$\rho\vec{q}''(n,t) + \zeta\vec{q}'(n,t) + \lambda_n\vec{q}(n,t) = \vec{B}(n,t) \qquad (6)$$

and

$$\epsilon Q^{IV}(n,s) - \kappa Q^{II}(n,s) - \lambda_n Q(n,s) = 0 \qquad (7)$$

As shown below, $\lambda_n = 0$ for $n = 0$. In this case, eq 6 gives a velocity autocorrelation function, which leads to the translational diffusion constant. For nonzero λ_n ($n \geq 1$), the inertia term can be neglected and eq 6 gives, under the usual approximations

$$\langle\vec{q}(n,t)\vec{q}(n,t+\tau)\rangle = \langle\vec{q}(n,t)^2\rangle \exp(-\tau/\tau_n) \qquad (8)$$

and

$$\tau_n = \zeta/\lambda_n \qquad (n = 1, 2, 3, \ldots) \qquad (9)$$

The elastic energy of the chain in the present model is given by

$$\langle V\rangle = \tfrac{1}{2}\sum_n \lambda_n\langle\vec{q}(n,t)^2\rangle \qquad (10)$$

Thus, from equipartition of energy, we have

$$\langle q_n^2\rangle \equiv \langle\vec{q}(n,t)^2\rangle = 3k_BT/\lambda_n \qquad (n = 1, 2, 3, \ldots) \qquad (11)$$

Equation 7 with free-end boundary conditions

$$Q^{II}(n,s) = \epsilon Q^{III}(n,s) - \kappa Q^{I}(n,s) = 0 \qquad \text{at} \qquad s = \pm L/2 \qquad (12)$$

determines the eigenvalues λ_n and eigenfunctions $Q(n,s)$. Putting

$$\begin{Bmatrix}\alpha\\ i\beta\end{Bmatrix} = [\kappa/2\epsilon \pm \{(\kappa/2\epsilon)^2 + \lambda_n/\epsilon\}^{1/2}]^{1/2} \qquad (13)$$

and

$$\alpha^2 - \beta^2 = \kappa/\epsilon \qquad (14)$$

where $\pm\alpha$ and $\pm i\beta$ are the roots of the characteristic equation to eq 7, we have the following transcendental equation:

$$1 - \cos(\beta L)\cosh(\alpha L) + \tfrac{1}{2}(y - 1/y)\sin(\beta L)\sinh(\alpha L) = 0 \qquad (15)$$

where $y \equiv (\beta/\alpha)^3$. The nth root, $\beta_n L$, of eq 15 gives

$$\lambda_n = \epsilon\beta_n^4 + \kappa\beta_n^2 \qquad (16)$$

or

$$3D\tau_n/L^2 = 4\gamma L/[(\beta_n L)^4 + (4\gamma L)(L^2/\langle R^2\rangle)(\beta_n L)^2] \qquad (n \geq 1) \qquad (17)$$

where D is the translational diffusion constant of the chain

$$D = k_BT/\Xi_{tr} \qquad \text{with} \qquad \Xi_{tr} = \zeta L \qquad (18)$$

because ζ was defined as the friction constant per unit length (see Appendix A). The first four $\beta_n L$ and three τ_n are shown in Figure 1 as functions of γL.[15] The eigenfunctions are given by

$$Q(0,s) = (1/L)^{1/2} \qquad (19a)$$

$$Q(n,s) = (c_n/L)^{1/2}\left[\frac{\sin(\beta_n s)}{\sin(\beta_n L/2)} + \left(\frac{\beta_n}{\alpha_n}\right)^2\frac{\sinh(\alpha_n s)}{\sinh(\alpha_n L/2)}\right] \qquad (19b)$$

(odd n)

$$Q(n,s) = (c_n/L)^{1/2}\left[\frac{\cos(\beta_n s)}{\cos(\beta_n L/2)} + \left(\frac{\beta_n}{\alpha_n}\right)^2\frac{\cosh(\alpha_n s)}{\cosh(\alpha_n L/2)}\right] \qquad (19c)$$

(even n)

where c_n's are normalization constants. The eigenfunction $Q(0,s)$ belonging to the eigenvalue $\lambda_0 = 0$ represents the translational motion of the center of resistance of the chain.

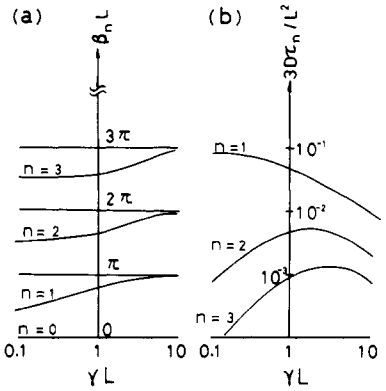

Figure 1. Graphic representation of numerical results: (a) $\beta_n L$ vs. γL; (b) $3D\tau_n/L^2$ vs. γL. Note that $\beta_1 L \rightarrow (48\gamma L)^{1/4}$ and $3D\tau_1/L^2 \rightarrow 1/12$ as $\gamma L \rightarrow 0$.

The eigenfunction $Q(1,s)$ in the stiff limit ($\gamma L \ll 1$) has the form

$$Q(1,s) = (12/L^3)^{1/2}s \tag{20}$$

which represents the rotational motion of a rod.

Now the field correlation function $g^{(1)}(\tau)$ is given by

$$g^{(1)}(\tau) = \exp(-D_0K^2\tau)S(\tau)/S(0) \tag{21a}$$

where

$$S(\tau) = (1/L^2)\int\int_{-L/2}^{L/2} J(s,s',\tau)\, ds\, ds' \tag{21b}$$

$$J(s,s',\tau) = \exp[-(K^2/6)\sum_n{}'\langle q_n^2\rangle \times \{Q(n,s)^2 + Q(n,s')^2 - 2Q(n,s)Q(n,s')\exp(-\tau/\tau_n)\}] \tag{21c}$$

and K is the length of the scattering vector.

Brief Note on Algorithm

For a given value of γL, we solve eq 15 to obtain $\alpha_n L$ and $\beta_n L$ and compute the normalization constant c_n's. Next, we take appropriate values of L and ζ (see Appendix A) to evaluate $\langle q_n^2\rangle$ and τ_n. To compute $S(\tau)$, we must carry out numerical double integration of eq 21b. Since $J(s,s',\tau)$ has a sharp ridge along the line $s = s'$ at $\tau = 0$ and a sharp peak at $s = s' = 0$ at $\tau = \infty$ (due to the strong contribution of the $n = 1$ mode), an adaptive quadrature algorithm based on Simpson's rule[16] was applied. (For testing of accuracy of numerical results, see Appendix B). Since it was difficult to determine beforehand how many modes should be added in eq 21c, we took n up to 1, 2, 4, 8, 12, 16, and 20 to see whether or not the computed profile of $g^{(1)}(\tau)$ changed appreciably as the number of added modes was increased. For the γL and K^2 values of present interest ($\gamma L \leq 0.5$, $L \simeq 1$ μm, and $K^2 \leq 12 \times 10^{10}$ cm^{-2}), n up to 8 was found to be large enough for the precision of numerical results for $g^{(1)}(\tau)$.

Stiff-Limit Behavior of Correlation Function

The asymptotic form of the smallest nonzero root of eq 15 in the stiff limit ($\gamma L \ll 1$) is given by

$$\beta_1 L = (48\gamma L)^{1/4} \quad \text{or} \quad \tau_1^{-1} = 36k_BT/\zeta L^3 \tag{22}$$

Now, let Ξ_{rot} be the friction constant of a rod rotating around its minor axis with angular velocity $\dot{\theta}$. Then we have in the long-rod limit

$$\Xi_{rot}\dot{\theta} = \text{torque} = 2\int_0^{L/2} (\zeta\, ds)\cdot(s\dot{\theta}) \times s \tag{23}$$

which leads to $\Xi_{rot} = \zeta L^3/12$ (see Appendix A), or

$$\tau_1^{-1} = 3\Theta \quad \text{with} \quad \Theta = k_BT/\Xi_{rot} \tag{24}$$[17]

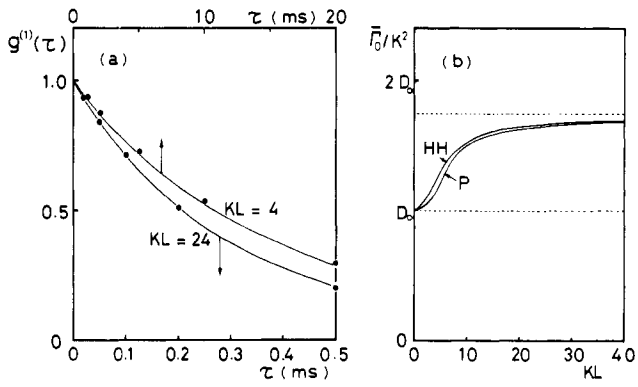

Figure 2. Correlation function profiles in the stiff limit. (a) Comparison of correlation function profiles predicted by our model at $\gamma L = 1 \times 10^{-3}$ (solid lines) and by Pecora's formula (dots). $L = 0.8$ μm, $KL = 4$ and 24, $D_0 = 2.35 \times 10^{-8}$ cm^2/s, $\Theta = 9D_0/L^2$, $\zeta = (4/3)k_BT/D_0L$ (see Appendix A), and $T = 20$ °C. (b) Apparent diffusion constants, $\bar{\Gamma}_0/K^2$, as a function of KL. HH, our model; P, from eq 28.

The field correlation function in the multiexponential form is given by

$$g^{(1)}(\tau) = J^{-1}\sum_{l\ \text{even}} P_l(KL)\exp[-(D_0K^2 + 3l\Theta)\tau] \tag{25}$$

where $J = \sum P_l(KL)$ ($\equiv S(0)$ of (B2) in Appendix B), $h \equiv KL/2\sqrt{6}$, and

$$P_l(KL) = \frac{2^l}{l!}\left[\frac{1}{h}\int_0^h z^l \exp(-z^2)\, dz\right]^2 \tag{26}$$

Equation 25 should be compared with Pecora's formula[18]

$$g^{(1)}(\tau) = J'^{-1}\sum_{l\ \text{even}} B_l(KL)\exp[-\{D_0K^2 + l(l+1)\Theta\}\tau] \tag{27}$$

where $J' = \sum B_l(KL)$. Although both the KL dependence of form factors and the l dependence of relaxation times are different in eq 25 and 27, numerical computation showed that eq 25 gave correlation function profiles practically indistinguishable from those computed with eq 27 for as large a KL value as 24 (Figure 2a).

The "theoretical" initial decay rate $\bar{\Gamma}_0$ of the correlation function given by Pecora's formula will be given by

$$\bar{\Gamma}_0/K^2 = D_0 + \Theta\frac{\sum l(l+1)B_l(KL)/K^2}{\sum B_l(KL)} \tag{28}$$

The $\bar{\Gamma}_0/K^2$ vs. KL relations for both the present model (see Appendix C) and Pecora's formula are shown in Figure 2b. The difference between the $\bar{\Gamma}_0/K^2$ values of both models is larger at smaller KL values, but the profiles of their correlation functions are similar because of the smaller contribution of the rotational mode. (As mentioned in the Model section, the model has some inconsistencies in the stiff limit. As to this, see Appendix D.)

Behavior of Correlation Function in the Semiflexible Region

To see the behavior of field correlation functions in the semiflexible region ($0 \ll \gamma L < 1$), correlation functions were computed for particular values of model parameters. We considered a long, thin filament, of which the D_0 value and the contour length were assumed to be 1.24×10^{-8} cm^2/s at 5 °C and 1.06 μm, respectively. The ζ value was calculated from the above D_0 value with eq A11 for $\Phi(p) = 1.1$ (see Appendix A). The only adjustable parameter in the present model was the value of γL, which was changed from 1×10^{-4} to 0.5.

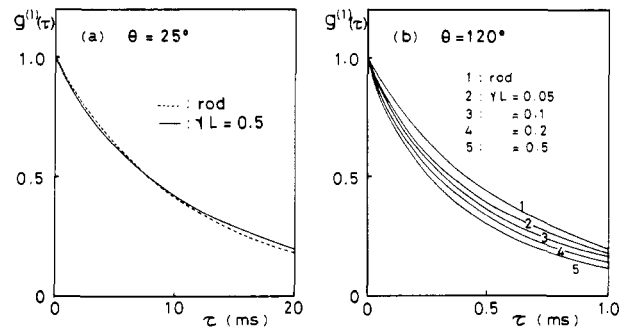

Figure 3. Correlation function profiles in the semiflexible region. $L = 1.06\ \mu m$, $D_0 = 1.24 \times 10^{-8}\ cm^2/s$ at 5 °C (both values equal those for a muscle thin filament; cf. application section), and $T = 5$ °C. The ζ value was evaluated from the D_0 value with eq A11 for $\Phi(p) = 1.1$. $n = 8$. (a) $\theta = 25°$ ($K^2 = 0.55 \times 10^{10}\ cm^{-2}$) and (b) $\theta = 120°$ ($K^2 = 8.8 \times 10^{10}\ cm^{-2}$).

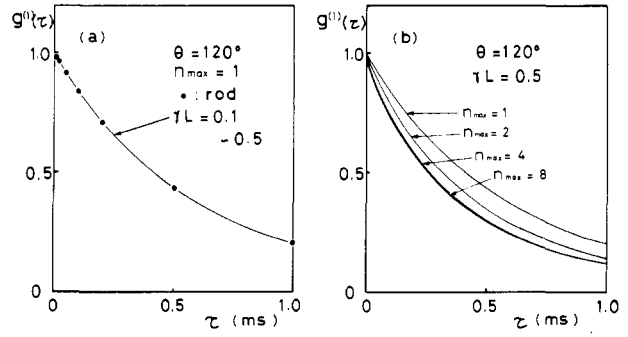

Figure 4. Effect of the number of modes taken in eq 21c on the correlation function profiles. Parameter values are the same as those in Figure 3. $\theta = 120°$. (a) $n_{max} = 1$ at varied γL values. (b) $n_{max} = 1$, 2, 4, and 8 at $\gamma L = 0.5$.

First, we computed the field correlation functions at different temperatures. So long as the γL value was held constant independent of temperature, the computed correlation functions scaled with the ratio of temperature to solvent viscosity, T/η, as they should. Therefore, we present here only the results at $T = 5$ °C.

Figure 3 shows results of simulation at the scattering angles $\theta = 25°$ (in a) and $\theta = 120°$ (in b) for different values of γL, taking the mode number n in eq 21c up to 8. At the scattering angle of 25°, computed correlation functions for different γL values are similar in shape. At the scattering angle of 120°, on the other hand, simulated correlation functions for different γL values look different from each other; the correlation functions for more flexible filaments decay faster. This means that, *if the γL value changes with temperature, the correlation functions do not scale with T/η.*

To see whether or not this nonscaling property of correlation functions at higher scattering angles came from the most dominant contribution of the $n = 1$ (rotational) mode, we computed the correlation functions at $\theta = 120°$, taking only $n = 1$ in eq 21c. The results shown in Figure 4a clearly indicate that the nonscaling property did not come from the rotational motion of the filaments. Figure 4b shows computed correlation functions at $\theta = 120°$ and $\gamma L = 0.5$, taking n in eq 21c up to 1, 2, 4, and 8.

Computed correlation functions were least-squares fitted to

$$\ln |g^{(1)}(\tau)| = \beta - \bar{\Gamma}\tau + \tfrac{1}{2}(\mu_2/\bar{\Gamma}^2)(\bar{\Gamma}\tau)^2 \qquad (29)$$

where $\bar{\Gamma}$ is the average decay rate and $\mu_2/\bar{\Gamma}^2$ the normalized dispersion.[19] In practical analysis, computed points up to τ_{max} were used, where $g^{(1)}(\tau_{max}) \sim 0.3$. Figure 5 shows the $\bar{\Gamma}$ vs. K^2 relations of computed correlation functions. As

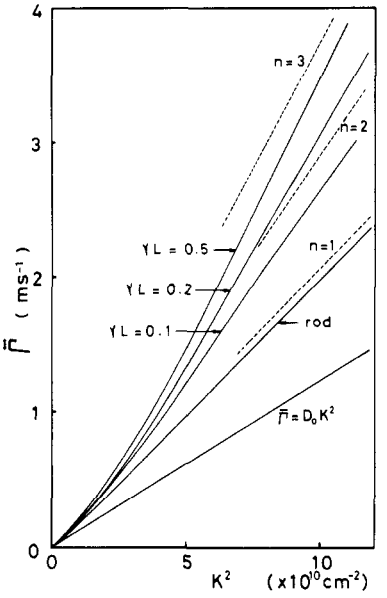

Figure 5. $\bar{\Gamma}$ vs. K^2 relations of computed correlation functions. Parameter values are the same as those in Figure 3. Dashed lines are given by eq 30 for $n = 1$, 2, and 3.

Table I
Numerical Values of Lateral Fluctuations[a]

	$\langle \delta_n^2 \rangle$, cm²		
γL	$n = 1$	$n = 2$	$n = 3$
0.1	780×10^{-12}	7.6×10^{-12}	1.1×10^{-12}
0.5	580×10^{-12}	32×10^{-12}	4.9×10^{-12}

[a] $(1/K^2)_{\theta=25°} = 182 \times 10^{-12}$ and $(1/K^2)_{\theta=120°} = 11 \times 10^{-12}$ (cm²). $L = 1\ \mu m$.

K^2 increases, the $\bar{\Gamma}$ vs. K^2 relation for a rigid rod approaches the line $\bar{\Gamma} = 1.68 D_0 K^2$, whereas those for semiflexible filaments with $\gamma L \gtrsim 0.1$ deflect upward from the line $\bar{\Gamma} = 1.68 D_0 K^2$. Since the ζ value in the present case was calculated with eq A11 for $\Phi(p) = 1.1$, the asymptotic form of $\bar{\Gamma}$ at large KL is derived from eq C6 as

$$\bar{\Gamma}_{(at\ KL \gg 1)} \simeq (1 + \tfrac{3}{4}\Phi(p)^{-1}n) D_0 K^2 \simeq (1 + 0.68n) D_0 K^2 \qquad (30)$$

where n is the number of internal modes. It is concluded that if the $\bar{\Gamma}$ value at finite K^2 becomes larger than the value given by eq 30 for a certain value of n, at least $n + 1$ internal modes of the filament are necessary for interpretation of the experimental $\bar{\Gamma}$ vs. K^2 relation.

The above results can qualitatively but physically be interpreted as follows. The mean-square-amplitude $\langle \delta^2 \rangle$ of the lateral fluctuations of the shape of the filament will be given by[20]

$$\langle \delta^2 \rangle = (1/L) \int_{-L/2}^{L/2} \langle \vec{r}(s,t)^2 \rangle\, ds = (1/L) \sum_n{}' \langle q_n^2 \rangle = \sum_n{}' \langle \delta_n^2 \rangle \qquad (31)$$

where

$$\langle \delta_n^2 \rangle = L^2 (3 D \tau_n / L^2) \qquad (32)$$

Table I lists some of $\langle \delta_n^2 \rangle$ values. It is known that the nth normal mode will contribute to the correlation function provided that

$$\langle \delta_n^2 \rangle \gtrsim 1/K^2 \qquad (33)$$

At $\theta = 25°$, we know from Table I that $\langle \delta_1^2 \rangle > 1/K^2$ and $\langle \delta_n^2 \rangle \ll 1/K^2$ for $n \geq 2$; that is, only the $n = 1$ mode

contributes appreciably to $g^{(1)}(\tau)$. At $\theta = 120°$, on the other hand, we know that $\langle\delta_1^2\rangle \gg 1/K^2$, $\langle\delta_2^2\rangle \gtrsim 1/K^2$, and $\langle\delta_3^2\rangle < 1/K^2$. In addition to the $n = 1$ mode, the $n = 2$ mode also contributes to the correlation functions. However, it should be noted that the contribution of the $n = 1$ mode almost saturates at this scattering angle as suspected from Figure 2b (note that $KL = 31$ for this particular scattering angle). If we remember that $3D\tau_1/L^2$ in Figure 1b changes little in the present range of γL, we can easily understand why the correlation functions in Figure 4a look alike. Likewise, if we remember that $3D\tau_n/L^2$ ($n \geq 2$) increases with increasing γL values, we can easily understand why the correlation functions with larger γL values decay faster than those with smaller γL values at $\theta = 120°$ (Figure 3b). Comparing $\langle\delta_1^2\rangle K^2 \simeq 3$ at $\theta = 25°$ with $\langle\delta_2^2\rangle_{\gamma L=0.5} K^2 \simeq 3$ at $\theta = 120°$, we can expect that the $n = 2$ mode contributes to the correlation function at $\theta = 120°$ by nearly the same amount that the $n = 1$ mode contributes at $\theta = 25°$.

The above explanation using eq 33 is inadequate to explain the result in Figure 4b. Equation 33 only says that P_n in the Introduction becomes appreciable at the K value where $K^2\langle\delta_n^2\rangle \sim 1$. The ratio P_n/τ_n is a true measure of the degree of contribution of the nth normal mode as already mentioned. Figure 4b clearly shows that the initial slope of the correlation function becomes larger as n increases but that the long-τ behavior is not much affected. (It is likely that the contribution of the $n \geq 3$ modes to the power spectrum is very small in this particular condition.)

Flexible-Limit Behavior of Correlation Function

It has been shown that the present model tends to the so-called Rouse–Zimm model in the flexible limit ($\gamma L \gg 1$).[3,4] In this limit, we have

$$\begin{aligned} Q(n,s) &= (2/L)^{1/2} \sin(n\pi s/L) \qquad \text{(odd } n\text{)} \\ Q(n,s) &= (2/L)^{1/2} \cos(n\pi s/L) \qquad \text{(even } n\text{)} \end{aligned} \tag{34}$$

$$\tau_n = \langle R^2\rangle/3D\pi^2n^2 \quad \text{and} \quad \langle q_n^2\rangle = \langle R^2\rangle L/\pi^2n^2 \tag{35}$$

where $\langle R^2\rangle = L^2/(\gamma L)$ is the end-to-end distance of the polymer. Since correlation functions at this limit are well-known,[7-10] we do not present our results here. (The present model will be applicable, for example, to the case of very large DNA molecules.)

Application of the Present Model

Newman and Carlson very recently reported the dynamic light-scattering data of solutions of fd virus and of intact thin filaments of scallop adductor muscle.[21] Because these particles seem to be good examples of semiflexible filaments, we try to apply our model to their dynamic light-scattering data.

1. fd Virus. The fd virus is one of the filamentous viruses specific for the male strain of *Escherichia coli*. Individual fd virus particles, observed under an electron microscope, showed slightly curved but nonuniform images. The contour length of these images corresponded to a virus length of 880 ± 15 nm.[22] The translational diffusion constant from dynamic light-scattering measurements and the rotational one from transient birefringence measurements were, after extrapolation to infinite dilution, $D_{25°C} = 2.58 \times 10^{-8}$ cm^2/s and $\Theta_{20°C} = 20.9$ s^{-1}, respectively, which corresponded to a virus length of 895 ± 20 nm and a diameter of 9 ± 1 nm.[11]

Newman and Carlson measured the intensity autocorrelation functions of light scattered from a solution of this fd virus at a wide range of scattering angles (or K values) and at different temperatures. Because their data of fd virus at different temperatures scaled with T/η, they concluded that fd virus is a rigid rod.[21] However, we found that, at K^2 larger than 1×10^{10} cm^{-2}, the experimental $\bar{\Gamma}$ values are very much larger than the values given by $\bar{\Gamma} = [1 + (3/4)\Phi(p)^{-1}]D_0K^2$ with $\Phi(p) = 1.2$. This suggests that another mode(s) has to be taken into account in simulation of correlation functions because the latter values are the upper bound for a rigid rod in the ideal case but the former values were at the finite concentration of 0.27 mg/mL and because fd virus is known to be highly stable and monodisperse.[22] Therefore, we computed the correlation functions at different γL values, adopting the above-quoted experimental values of $L = 895$ nm and D_0 and Θ after T/η correction to 5 °C. The ζ value was calculated from the above D_0 value and eq A11 for $\Phi(p) = 1.2$. Profiles of computed correlation functions for γL values smaller than 1×10^{-2} were practically the same as those computed with Pecora's formula for a rigid rod. The $\bar{\Gamma}$ vs. K^2 relations are shown in Figure 6. Computed correlation functions deviated slightly from single-exponential decay curves as indicated by $\mu_2/\bar{\Gamma}^2$ values ranging from 0.1 to 0.3. The results in Figure 6 strongly suggest that the γL value of fd virus is about 0.1.

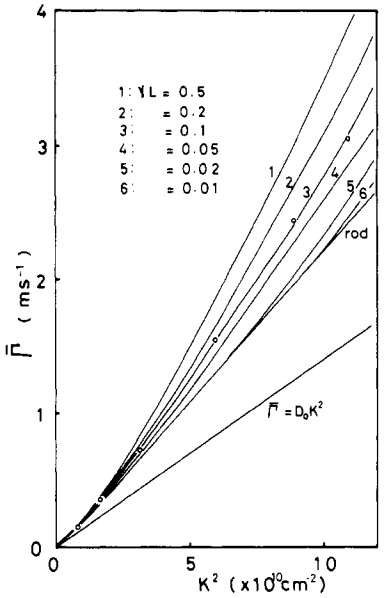

Figure 6. $\bar{\Gamma}$ vs. K^2 relations of computed correlation functions for fd virus at 5 °C and of experimental ones after T/η scaling to 5 °C. Experimental points (○) were from Figure 2B of ref 21. Parameter values are $L = 0.895$ μm, $D_0 = 1.42 \times 10^{-8}$ cm^2/s, and $\Theta = 13.1$ s^{-1} at 5 °C. The ζ value was evaluated from the D_0 value with eq A11 for $\Phi(p) = 1.2$.

Newman et al. stated that there was no evidence of the flexibility of the fd particle in solution because the birefringence decay data were described by a single-exponential function and because the Θ values were independent of the applied field strength.[11] Actually, the value of $3D\tau_1/L^2$ varies little as long as the γL value is smaller than 0.2. The value of $3D\tau_2/L^2$ at $\gamma L = 0.1$ gives $\tau_2^{-1} = 13 \times 10^3$ s^{-1}, which is 2 orders of magnitude larger than $6\Theta = 125$ s^{-1}. It is rather difficult to detect the small contribution of this fast-relaxing component in the transient birefringence decay data. Here we again see a sensitive contribution of components having shorter time constants to light-scattering correlation functions at higher scattering angles. Although a quantitative analysis of light-scattering data at higher scattering angles is very difficult, our method of analysis seems to be powerful for seeing gross properties of huge molecules.

2. Muscle Thin Filament. A muscle thin filament is composed mainly of fibrous actin (F-actin) decorated with

other muscle proteins such as tropomyosin and troponin and is about 1 μm in length. F-actin and its complexes with other muscle proteins have been extensively studied by means of dynamic light scattering,[3,21,23-27] electron microscopy,[28] dark-field optical microscopy,[29] fluorescence depolarization,[30,31] and electrooptics.[32-34] The values of the flexibility parameter (γ) of F-actin and its complexes with other muscle proteins under various solvent conditions are on the order of 0.1 μm^{-1}, and F-actin can be considered as an example of semiflexible filaments.

Newman and Carlson very recently reported the dynamic light-scattering data of a solution of intact thin filaments from scallop adductor muscle.[21] This thin filament is composed of F-actin and only tropomyosin. Since we are going to try to analyze their data on the basis of our model, we at first summarize their results in some detail in the following.

(a) The low-angle (θ = 10–25°) intensity autocorrelation functions of scattered light were independent of concentration (0.08–1.3 mg/mL), scaled with the ratio of temperature to solvent viscosity (T/η), over a range of T = 4–45 °C, and yielded a value for the translational diffusion constant ($D_{5°C}$ = 1.24 × 10^{-8} cm^2/s) which corresponded to a filament length of 1.06 μm. High-angle (θ = 60–150°) data did not scale with the ratio T/η, and the average decay constant, $\bar{\Gamma}$, scaled by T/η became larger as temperature was increased from 5 to 44 °C. Quantitative sodium dodecyl sulfate–polyacrylamide gel electrophoresis showed that at high temperature (T > 35 °C), tropomyosin completely dissociated from native thin filaments.

(b) The change in the concentration of salt in solution from 0.05 to 0.6 M NaCl did not affect the $\bar{\Gamma}$ values at θ = 30°, but at higher angles the $\bar{\Gamma}$ values became larger and were similar to those observed for samples heated to 40–45 °C. It was also shown that tropomyosin completely dissociated from F-actin in 0.6 M NaCl solution.

(c) The absence of T/η scaling for native thin filaments could not be explained by a number of possible explanations, such as multiple scattering, change in length distribution of the filaments, interaction between filaments, thermal convection, and the scattering of free tropomyosin. Together with the experimental result in 0.6 M salt solution, they concluded that the removal of tropomyosin was responsible for the increase of $\bar{\Gamma}$ values, which they had attributed to a change in the flexibility of thin filaments.

Their conclusion, i.e., the last several lines in c, may be true, but a more quantitative analysis seems to be necessary. They stated in their paper that there was as yet no complete theory for analyzing their data in detail. Although the present model is not complete, it is worthwhile to apply the model to their data.

The statements given before can be applied, at least qualitatively, to the data of the thin filaments as they are. The behavior of simulated results shown in Figures 3 and 5 are compatible with the experimental results a and b summarized above. The results in Figure 4 suggest that the observed nonscaling property does not come from the rotational motion of the filaments. This is different from their expectation that no adequate fit of our model[4] to their data comes from "the neglect of contributions to the correlation function from rotational diffusion".

But our simulation given before does not agree *quantitatively* with the experimental data for thin filaments. Figure 7a shows experimental $\bar{\Gamma}$ vs. K^2 relations taken from ref 21. Experimental $\bar{\Gamma}$ values for the thin filament without tropomyosin (open symbols) are larger at larger K^2 values than the theoretical ones for a stiff rod (curve 1, taken from Figure 5). If we take into account a slight flexibility of the

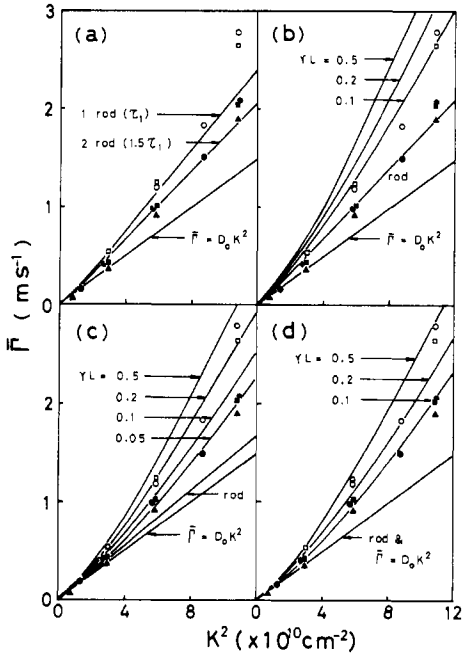

Figure 7. $\bar{\Gamma}$ vs. K^2 relations for muscle thin filaments after T/η scaling to 5 °C. (a) Experimental points were from Figures 2A and 3 of ref 21: (●) measured at 5.5 °C and (○) at 44 °C, both at 1.26 mg/mL thin filaments in 0.05 M NaCl; (▲) measured at 5 °C and 2.3 mg/mL in 0.05 M NaCl; (■) measured at 5 °C and 1.15 mg/mL in 0.05 M NaCl; (□) measured at 5 °C and 1.15 mg/mL in 0.6 M NaCl. (○, □) Thin filament without tropomyosin; (●, ■, ▲) thin filament with tropomyosin. Curve 1 is the $\bar{\Gamma}$ vs. K^2 relation for a stiff rod taken from Figure 5, and curve 2 the $\bar{\Gamma}$ vs. K^2 relation for a stiff rod assuming τ_1 = 1.5 times the theoretical τ_1 (see text). (b) $\bar{\Gamma}$ vs. K^2 relations of computed correlation functions at 5 °C. Parameter values are the same as those in Figure 3 except that τ_1 = 1.5 times the theoretical τ_1 (see text). (c) The same as in (b) except that τ_1 = 5 times the theoretical τ_1. (d) The same as in (b) except that τ_1 = ∞.

thin filament, a rough fit will be obtained between $\bar{\Gamma}$ vs. K^2 relations of experimental and simulated results. On the other hand, experimental $\bar{\Gamma}$ values for the thin filament with tropomyosin (closed symbols) are definitely smaller than the theoretical ones (curve 1). This is in marked contrast to the case of fd virus mentioned before. In this case, we have to reduce the contribution to the $\bar{\Gamma}$ value from, at least, rotational diffusion. In fact, the low-angle data in the insert of Figure 2A of ref 21 show that the $\bar{\Gamma}$ vs. K^2 relation is straight up to $K^2 \simeq 0.7 \times 10^{10}$ cm^{-2} (or $KL \simeq 8.4$) independent of the concentrations (0.08–1.3 mg/mL; see a in the above summary). Consulting Figure 2b, we guess from these low-angle data that the contribution to the $\bar{\Gamma}$ value from rotational diffusion is very strongly suppressed in this particular example. In addition to this, a 1:1 dilution of a 2.3 mg/mL solution of thin filaments substantially increased the $\bar{\Gamma}$ values at higher scattering angles (▲ → ■ in Figure 7a). This suggests that the contribution to the $\bar{\Gamma}$ values from the n = 2 mode, for example, is somewhat suppressed. From Table I, we know that $\langle \delta_1^2 \rangle^{1/2}$ = 280 nm at γL = 0.1. This means that the average amplitude of the n = 1 mode is only slightly smaller than the average distance between the center of mass of filaments at the concentration of 1 mg/mL thin filaments. The rotational fluctuation of the thin filament is supposed to be strongly suppressed under such a condition, whereas small fluctuations of flexing motions may not be. Taking these considerations into account, we at first determined the increased τ_1 value so that the simulated correlation functions in the stiff limit gave the experimental $\bar{\Gamma}$ vs. K^2 relation of the thin filament with

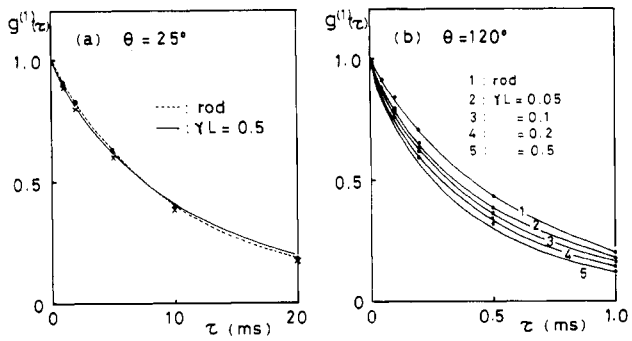

Figure 8. Profiles of computed correlation functions. The parameter values are the same as those in Figure 3. (—, ---) From Figure 3; (●, ×) based on eq D7 with eq A8 for the Θ value. (a) (●) At $\gamma L = 0.0$ (rod); (×) at $\gamma L = 0.5$. (b) Dots from top to bottom at each τ value show computed points at $\gamma L = 0.0$ (rod), 0.05, 0.1, 0.2, and 0.5, respectively.

tropomyosin. The 50% increase of τ_1 resulted in a rough fit as shown in Figure 7a (curve 2).

Using the above modified value of τ_1 (i.e., 1.5 times the theoretical τ_1) and keeping both $\langle q_n^2 \rangle$ for $n \geq 1$ and τ_n for $n \geq 2$ theoretical ones, we again computed the correlation functions for different γL values. The results in Figure 7b suggest that the γL value of the thin filament without tropomyosin is at least 0.1, on the assumption that the thin filament with tropomyosin is very stiff. Much better reconstruction of $\bar{\Gamma}$ vs. K^2 relations for the thin filaments with and without tropomyosin is possible if we assume τ_1 = 5 times the theoretical τ_1 in Figure 7c and $\tau_1 = \infty$ in Figure 7d.

From the viewpoint of curve fitting, the result in Figure 7c or Figure 7d is better than the others. The γL values are about 0.05 and 0.2 in Figure 7c and about 0.1 and 0.4 in Figure 7d for the thin filaments with and without tropomyosin, respectively. The change in the filament flexibility is expected to come from not only the removal of tropomyosin from F-actin but also loosening of the F-actin structure at high temperature or at high ionic strengths. These values of γL are comparable with those of previous studies by various different techniques. From the limited data available in the literature,[21] however, it is not easy to *completely* rule out the possibility that the lack of scaling came mainly from the change in τ_1 values under different environmental conditions as shown in Figure 7a. This possibility makes the analysis of data on thin filaments somewhat ambiguous compared with that for the case of fd virus mentioned before. It seems necessary to make a more detailed study in order to determine unambiguously the flexibility parameter of the muscle thin filament from light-scattering spectra.

Conclusion

Our theory is essentially based on a free-draining wormlike chain model of polymer dynamics, and, moreover, the model in the stiff limit includes some inconsistencies within itself. However, the dynamic light-scattering spectrum in the stiff limit of our theory is practically indistinguishable from that predicted by the rigorous theory for a rod. The present computations made it possible to interpret both the larger $\bar{\Gamma}$ values of the fd virus than those of a rigid rod and the change of the dynamic light-scattering spectrum of muscle thin filaments with and without tropomyosin in terms of the filament flexibility. The present results will serve as a guiding principle in the analysis of dynamic light-scattering data of very long, semiflexible filaments until a better theory based on a more realistic model appears.

Acknowledgment. We thank Professor F. D. Carlson and his associates for sending us some of their original data.

Appendix A. Evaluation of the ζ Value

We consider the frictional properties (Ξ_{tr} and Ξ_{rot}) of a semiflexible rod. For this purpose, we first examine the friction constants of a rigid rod. For the axial ratio $p \gg 1$, we have

$$\Xi_{tr} = 3\pi\eta L/[\ln (2p) - \delta] \tag{A1}$$

$$\Xi_{rot} = \pi\eta L^3/3[\ln (2p) - \xi] \tag{A2}$$

where $\delta = 0$ and $\xi = 0.5$ (Perrin's formulas)[35] or $\delta = -5.8/[\ln (2p)]^2 + 4.15/\ln (2p) - 0.017$ and $\xi = 1.45 - 7.5[1/\ln (2p) - 0.27]^2$ (Broersma's formulas)[36] and other notations have their usual meanings. From eq A1 and A2, we have

$$\Xi_{rot} = \Xi_{tr}\frac{L^2}{9}\Phi(p) \qquad \text{with} \qquad \Phi(p) = \frac{\ln (2p) - \delta}{\ln (2p) - \xi} \tag{A3}$$

For p values of present interest ($p \sim 100$), the ratio $\Phi(p)$ has values of 1.1 (Perrin) and 1.2 (Broersma).

In the stiff limit, the friction constant ζ (and also the translational diffusion constant D in eq 18) in our model should be regarded as that of the "sideway" translation of a filament. Let subscripts o and || mean "overall" and "lengthway", respectively. Then we have

$$D_o = (2D + D_{||})/3 = (4/3)D$$

or

$$\Xi_{tr,o} = \zeta_o L = (3/4)\zeta L \tag{A4}$$

where $D_{||} = 2D$ or $\zeta_{||} = \zeta/2$ was assumed[35-37] and D is given by eq 18. From eq A4 and 24, we have

$$\Xi_{rot} = \Xi_{tr,o}(L^2/9) \tag{A5}$$

which differs from eq A3 only by the factor $\Phi(p)$.

Our model does not include any sophisticated problem of hydrodynamic interaction, so that our ζ should be replaced by appropriate expressions. For example, from eq A4 and A1 and from eq 24 and A2, we have

$$\zeta_{tr} = 4\pi\eta/[\ln (2p) - \delta] \tag{A6}$$

$$\zeta_{rot} = 4\pi\eta/[\ln (2p) - \xi] \tag{A7}$$

For a semiflexible rod, whose γL value is not very much smaller than unity, friction constants would differ from those for a rigid rod. However, since we consider only the cases of $\gamma L \leq 0.5$, changes in friction constants with γL values may be neglected.

When the experimental Θ value is available, evaluation of the ζ value can be made by use of

$$\Theta = 12k_BT/\zeta L^3 \tag{A8}$$

or

$$\Theta = (12k_BT/\zeta L^3)\Phi(p)^{-1} \tag{A9}$$

When only the experimental D_o value is available, the evaluation of the ζ value will be made by use of

$$D_o = (4/3)k_BT/\zeta L \tag{A10}$$

or

$$D_o = [(4/3)k_BT/\zeta L]\Phi(p) \tag{A11}$$

When we assume $\Theta = 3k_BT[\ln (2p) - \xi]/\pi\eta L^3$ and $D_o = k_BT[\ln (2p) - \delta]/3\pi\eta L$, both eq A8 and A11 give $\zeta = \zeta_{rot}$ in eq A7, and both eq A9 and A10 give $\zeta = \zeta_{tr}$ in eq A6. If there is a reasonable indication that the experimental

D_0 and/or Θ value is affected by nonideality of the solution, eq A6 or A7 should be used for the evaluation of the ζ value.

Appendix B. Test of the Computer Program

To test the computer program we wrote for double integration in eq 21b, numerical results at special points were compared with the following results.

(i) At $\gamma L \ll 1$ (Stiff Limit)

Since eq 21c is reduced to

$$J(s,s',\tau) = \exp[-(K^2/6)(s^2 + s'^2 - 2ss'e^{-\tau/\tau_1})] \quad \text{(B1)}$$

we have

$$S(0) = (\pi^{1/2}/2h)\ \text{erf}\ (2h) - [1 - \exp(-4h^2)]/(4h^2) \quad \text{(B2)}$$

and

$$S(\infty) = \pi[\text{erf}\ (h)/(2h)]^2 \qquad (\equiv P_0(KL) \text{ in eq } 26) \quad \text{(B3)}$$

where $h \equiv KL/2\sqrt{6}$ and

$$\text{erf}\ (u) = (2/\pi^{1/2})\int_0^u \exp(-z^2)\ dz \quad \text{(B4)}$$

(ii) At $\gamma L \gg 1$ (Flexible Limit)

In this limit, we have the well-known relations

$$S(0) = (2/X^2)(e^{-X} - 1 + X) \qquad (\equiv P(X) \text{ in ref } 2) \quad \text{(B5)}$$

and

$$S(\infty) = (\pi/X)\exp(-X/6)[\text{erf}\ (X^{1/2}/2)]^2 \qquad (\equiv P_0(X) \text{ in ref } 2) \quad \text{(B6)}$$

where $X \equiv K^2L^2/6\gamma L$. The above special values of $S(\tau)$ can be evaluated without numerical integration.

(iii) At Arbitrary Values of γL

The results of numerical double integration at $\tau = \infty$ were compared with those of the following single integration:

$$S(\infty) = \left[(2/L)\int_0^{L/2} \exp\{-(K^2/6)\sum_n{}'\langle q_n^2\rangle Q(n,s)^2\}\ ds\right]^2 \quad \text{(B7)}$$

Appendix C. Values of $\bar{\Gamma}/K^2$ at Large KL

Noting that $\langle q_n^2\rangle/\tau_n = 3k_BT/\zeta$, we have from eq 21

$$-\frac{d}{d\tau}\ln g^{(1)}(\tau)|_{\tau=t} = D_0K^2 + \frac{k_BT}{\zeta}K^2\sum_n{}' \exp(-t/\tau_n)f(KL,n,t) \quad \text{(C1)}$$

where

$$f(KL,n,t) = (1/L^2)\int\int_{-L/2}^{L/2} Q(n,s)Q(n,s')J(s,s',t)\ ds\ ds'/S(0) \quad \text{(C2)}$$

The "theoretical" initial decay rate $\bar{\Gamma}_0$ of $g^{(1)}(\tau)$ is defined by eq C1 with $t = 0$

$$\bar{\Gamma}_0/K^2 = D_0 + (k_BT/\zeta)\sum_n{}' f(KL,n,0) \quad \text{(C3)}$$

As already mentioned, $J(s,s',0)$ has a very sharp ridge along $s = s'$ for very large KL values, and we have an approximation

$$J(s,s',0) \to LS(0)\delta(s - s') \qquad \text{for} \qquad KL \gg 1 \quad \text{(C4)}$$

Then we have for arbitrary values of γL

$$f(KL,n,0) \to (1/L)\int_{-L/2}^{L/2} Q(n,s)^2\ ds = 1/L \quad \text{(C5)}$$

from which we have the limiting value

$$\bar{\Gamma}_0/K^2 \to D_0 + k_BT/b$$

with

$$b \equiv \zeta L/\sum_n{}' 1 = \zeta L/n \quad \text{(C6)}$$

As has been pointed out,[38] the theoretical $\bar{\Gamma}_0$ value depends on the degree of freedom (or mode number n) *at the outset*. In the stiff limit, the number of modes is, of course, 2; i.e., $n = 0$ for translation and $n = 1$ for rotation. Therefore we have $n = 1$ in eq C6 or

$$\bar{\Gamma}_0/K^2 \to D_0 + k_BT/\zeta L \qquad (\text{at } \gamma L \ll 1) \quad \text{(C7)}$$

In the limiting cases of γL values, $f(KL,n,0)$ can be evaluated analytically.

(i) At $\gamma L \ll 1$ (Stiff Limit)

From eq 20 and B1, we have

$$f(KL,1,0) = \frac{1}{L}\left[1 + \frac{1 - 4h^2 - e^{-4h^2}}{S(0)8h^4}\right] \quad \text{(C8)}$$

where $S(0)$ is given by eq B2 and $h \equiv KL/2\sqrt{6}$ as before.

(ii) At $\gamma L \gg 1$ (Flexible Limit)

From eq 34 and 35, we have

$$f(X,n,0) = (1/L)(e^{-X} + X - 1)^{-1}[(X - 1)I_1(n) - I_2(n)] \quad \text{(C9)}$$

where $X \equiv K^2L^2/6\gamma L$ as before and

$$I_1(n) = [1 + (n\pi/X)^2]^{-1}[1 - (-1)^n e^{-X}] \quad \text{(C10)}$$

$$I_2(n) = [1 + (n\pi/X)^2]^{-1}\{-(-1)^n Xe^{-X} + [1 - (n\pi/X)^2]I_1(n)\} \quad \text{(C11)}$$

The "experimental" initial decay rate $\bar{\Gamma}$, on the other hand, will be given by eq C1 with $t = T$ (the channel width of the correlator used)

$$\bar{\Gamma}/K^2 = D_0 + (k_BT/\zeta)\sum_n{}' \exp(-T/\tau_n)f(KL,n,T) \quad \text{(C3')}$$

The factor $\exp(-T/\tau_n)$ will decrease the contributions of extra degree of freedom. If we assume $T = \tau_1/\alpha$, we have $\exp(-T/\tau_n) = \exp(-n^2/\alpha)$ for the flexible limit ($\gamma L \gg 1$). Then we have $\sum_n{}' \exp(-n^2/\alpha) = 2.3$ for $\alpha = 10$, 3.4_6 for $\alpha = 20$, and 5.1 for $\alpha = 40$, which are much smaller than $\sum_n{}'1$.

Appendix D. A Note on the Stiff Limit of the Model

The most general formulation of the potential energy of a chain given by Soda[13] has the form

$$V = \int_{-L/2}^{L/2}\left[\frac{\epsilon}{2}\left\{\left(\frac{\partial^2\vec{r}}{\partial s^2}\right)^2 - \left(\vec{t}\cdot\frac{\partial^2\vec{r}}{\partial s^2}\right)^2\right\} + \frac{\kappa}{2}\left\{\left|\frac{\partial\vec{r}}{\partial s}\right| - 1\right\}^2\right] ds \quad \text{(D1)}$$

where $\vec{t}$ is a unit vector pointing in the direction of the tangent vector to the chain at given s and t. Equation D1 becomes eq 1 provided that

$$\left(\frac{\partial^2\vec{r}}{\partial s^2}\right)^2 \gg \left(\vec{t}\cdot\frac{\partial^2\vec{r}}{\partial s^2}\right)^2 \quad \text{and} \quad \left\{\left|\frac{\partial\vec{r}}{\partial s}\right| - 1\right\}^2 \simeq \left(\frac{\partial\vec{r}}{\partial s}\right)^2 \quad \text{(D2)}$$

The first inequality in eq D2 will be satisfied when the curvature of the chain is caused mainly by bending. The second condition will be realized when longitudinal deformations are large. These conditions are not compatible.[39] Therefore, we have to consider carefully the result of the Harris–Hearst (HH) model in the stiff limit.

To see the property of the HH model in the stiff limit, we at first consider a model situation where a rod is assumed to be nonstretchable but bendable. In this case, $\partial^2\vec{r}/\partial s^2$ is perpendicular to $\vec{t}$ and $|\partial\vec{r}/\partial s| - 1 = 0$, and we have

$$\rho(\partial^2\vec{r}/\partial t^2) + \zeta(\partial\vec{r}/\partial t) + \epsilon(\partial^4\vec{r}/\partial s^4) = \vec{A}(s,t) \quad \text{(D3)}$$

This equation is more realistic for a stiff rod than eq 2 is. By simply putting $\kappa = 0$ and hence $\alpha = \beta$, eigenvalues and eigenfunctions of eq D3 can be obtained from relevant expressions of the HH model in the Model section.[3,4] The only thing we have to notice here is

$$\beta_1 L = 0 \qquad \text{and hence} \qquad \lambda_1 = 0 \quad \text{(D4)}$$

In the limit of $\gamma L \to 0$, we have only two modes in eq 5:

$$\vec{r}(s,t) = \vec{r}_G(t) + s\vec{t}(t) \quad \text{(D5a)}$$

$$\vec{A}(s,t) = \vec{F}(t)/L + s\vec{T}(t) \times (12/L^3) \quad \text{(D5b)}$$

where $\vec{r}_G(t)$ is the position vector of the center of mass of the rod, $\vec{t}(t)$ is the unit vector parallel to the major axis of the rod, $\vec{F}(t) = \int\vec{A}(s,t)\,ds$ is the random force acting on $\vec{r}_G(t)$, and $\vec{T}(t) = \int\vec{A}(s,t)s\,ds$ is the random torque acting on the rod. Then eq D3 gives

$$m\vec{r}_G''(t) + \Xi_{tr}\vec{r}_G'(t) = \vec{F}(t) \quad \text{(D6a)}$$

$$I\vec{t}''(t) + \Xi_{rot}\vec{t}'(t) = \vec{T}(t) \quad \text{(D6b)}$$

where $m = \rho L$, $\Xi_{tr} = \zeta L$ (but see Appendix A), $I = \rho L^3/12$ (the moment of inertia of the rod around its minor axis), and $\Xi_{rot} = \zeta L^3/12$. Equation D6a represents the translational Brownian motion. Equation D6b represents the rotational Brownian motion because the time derivative of the unit vector $\vec{t}(t)$ can be regarded as the angular velocity of the rod rotating around its minor axis. From these considerations, we have a good approximation for a slightly bendable but not stretchable rod as

$$J(s,s',\tau) = \langle e^{i\vec{K}\cdot[s\vec{t}(t)-s'\vec{t}(t+\tau)]}\rangle_{rot} \exp[-(K^2/6)\sum_n{}''\langle q_n{}^2\rangle \times \{Q(n,s)^2 + Q(n,s')^2 - 2Q(n,s)Q(n,s')e^{-\tau/\tau_n}\}] \quad \text{(D7)}$$

where $\sum_n{}''$ is the summation over n except $n = 0$ and 1. The average, $\langle\cdots\rangle_{rot}$ can be evaluated following Pecora's original method. When the rod is slightly bendable ($\gamma L \neq 0$), the bending motion modifies Pecora's result.[18]

The doubly degenerate eigenvalues ($\beta_0 L = \beta_1 L = 0$) in the above model split into different values ($\beta_0 L = 0$ and $\beta_1 L \neq 0$) in the HH model, and we have $\beta_1 L = (48\gamma L)^{1/4}$, which actually goes to zero as $\gamma L \to 0$, but both τ_1 and $\langle q_1{}^2\rangle$ tend to finite values as $\gamma L \to 0$. This comes solely from the presence of the κ term in eq 2. The $n = 1$ mode of the HH model in the stiff limit is not the rotational one because this mode produces potential energy through the stretch/contraction term in eq 1 (note that $\partial Q(1,s)/\partial s \neq 0$ but $\partial^2 Q(1,s)/\partial s^2 = 0$). The rod is always pointing in the initial direction and is stretched and contracted in the manner that $Q(1,s)$ represents. This deformed conformation relaxes with the time constant $\tau_1 = 1/3\Theta$. Such a nonphysical property originates from the fact that s in the HH model is not a measure of distance on the contour but essentially a numbering parameter as in a discrete model.[13,14] The integral over s from $-L/2$ to $L/2$ means the integral over all chain elements. However, if we regard s as the true coordinate on the contour, we have a nice analogy with eq D6b. From eq 6 and $\lambda_1 = 36k_BT/L^3$ at $\gamma L \to 0$, we have

$$I\vec{t}''(t) + \Xi_{rot}\vec{t}'(t) + 3k_BT\vec{t}(t) = \vec{T}(t) \quad \text{(D8)}$$

Equation D8 has the "restoring force" $|3k_BT\vec{t}(t)| = 3k_BT$. This restoring force in the HH model plays a role of entropy force in rotational diffusion. From eq D8 we have $\langle\vec{t}(t)\vec{t}(t+\tau)\rangle = (1/3)\exp(-3\Theta\tau)$. If $z(t) \equiv \vec{K}\cdot[\vec{t}(t)s - \vec{t}(t+\tau)s']$ is assumed to be a Gaussian random variable, it holds that

$$\langle e^{iz(t)}\rangle = e^{-\langle z^2\rangle/2} = \exp[-(K^2/6)(s^2 + s'^2 - 2ss'e^{-3\Theta\tau})] \quad \text{(D9)}$$

This is certainly a mathematical trick. However, as far as the large KL values are concerned, the above trick works well as shown in Figure 2. For small KL values, eq D7 should be used.

In Figure 8, the profiles of computed correlation functions based on eq D7 are compared with the previous ones in Figure 3. Since the τ_n values for eq D3 at finite γL values are larger than the corresponding ones for eq 2, the computed correlation function decays more slowly than that on the HH model. From Figure 8, however, the profiles of correlation functions based on both models are indistinguishable from each other at least at $\gamma L \lesssim 0.2$. From the results in Figures 2 and 8, it is suggested that the HH model is not too bad for simulation of dynamic light-scattering spectrum for very long, semiflexible filaments.

References and Notes

(1) Pecora, R. *J. Chem. Phys.* **1965**, *43*, 1562.
(2) Pecora, R. *J. Chem. Phys.* **1968**, *49*, 1032.
(3) Fujime, S. *J. Phys. Soc. Jpn.* **1970**, *29*, 751.
(4) Fujime, S.; Maruyama, M. *Macromolecules* **1973**, *6*, 237.
(5) de Gennes, P. G. *Physics* **1967**, *3*, 37.
(6) Dubois-Violette, E.; de Gennes, P. G. *Physics* **1967**, *3*, 181.
(7) Saleh, B.; Hendrix, J. *Chem. Phys.* **1976**, *12*, 25.
(8) Hendrix, J.; Saleh, B.; Gnädig, K.; De Maeyer, L. *Polymer* **1977**, *18*, 10.
(9) Lin, S.-C.; Schurr, J. M. *Biopolymers* **1978**, *17*, 425.
(10) Thomas, J. C.; Allison, S. A.; Schurr, J. M.; Holder, R. D. *Biopolymers* **1980**, *19*, 1451.
(11) Newman, J.; Swinney, H. L.; Day, L. A. *J. Mol. Biol.* **1977**, *116*, 593.
(12) Kuroda, K.; Kageyama, M.; Maeda, T.; Fujime, S. *J. Biochem.* **1979**, *85*, 21.
(13) Soda, K. *J. Phys. Soc. Jpn.* **1973**, *35*, 866.
(14) Harris, R. A.; Hearst, J. E. *J. Chem. Phys.* **1966**, *44*, 2595.
(15) Graphic representation of $3D\tau_1/L^2$ in ref 4 is incorrect.
(16) Davis, P. J.; Rabinowitz, P. "Methods of Numerical Integration"; Academic Press: New York, 1975.
(17) Loh (Loh, E. *Biopolymers* **1979**, *18*, 2569) equated his experimental Θ value to our τ_1^{-1}. This seems to be wrong and eq 24 should be used.
(18) Pecora, R. *J. Chem. Phys.* **1968**, *49*, 4126.
(19) Koppel, D. E. *J. Chem. Phys.* **1972**, *57*, 4814.
(20) Fujime, S. *J. Phys. Soc. Jpn.* **1971**, *31*, 1805.
(21) Newman, J.; Carlson, F. D. *Biophys. J.* **1980**, *29*, 37.
(22) Frank, H.; Day, L. A. *Virology* **1970**, *42*, 144.
(23) Fujime, S.; Ishiwata, S. *J. Mol. Biol.* **1971**, *62*, 251.
(24) Ishiwata, S.; Fujime, S. *J. Mol. Biol.* **1972**, *68*, 511.
(25) Carlson, F. D.; Fraser, A. B. *J. Mol. Biol.* **1974**, *89*, 273.
(26) Fraser, A. B.; Eisenberg, E.; Kielley, W. W.; Carlson, F. D. *Biochemistry* **1975**, *14*, 2207.
(27) Maeda, T.; Fujime, S. *J. Phys. Soc. Jpn.* **1977**, *42*, 1983.
(28) Takebayashi, T.; Morita, Y.; Oosawa, F. *Biochim. Biophys. Acta* **1977**, *492*, 357.
(29) Nagashima, H.; Asakura, S. *J. Mol. Biol.* **1980**, *136*, 169.
(30) Yanagida, T.; Oosawa, F. *J. Mol. Biol.* **1978**, *126*, 507.
(31) Yanagida, T.; Oosawa, F. *J. Mol. Biol.* **1980**, *140*, 313.
(32) Umazume, Y.; Fujime, S. *Biophys. J.* **1975**, *15*, 163.
(33) Yoshino, S.; Umazume, Y.; Natori, R.; Fujime, S.; Chiba, S. *Biophys. Chem.* **1978**, *8*, 317.
(34) Yoshino, S.; Fujime, S. "Muscle Contraction: Its Regulatory Mechanisms"; Ebashi, S., et al., Eds.; Japan Scientific Societies Press (Tokyo)/Springer-Verlag (Berlin): 1980; p 181.

(35) Perrin, F. *J. Phys. Radium* **1934**, *5*, 497. *Ibid.* **1936**, *7*, 1.
(36) Broersma, S. *J. Chem. Phys.* **1960**, *32*, 1626, 1632. The forms of δ and ξ as functions of p are from eq 3 and 4 in ref 11.
(37) Lamb, H. "Hydrodynamics", 6th ed.; Cambridge University Press: New York, 1932; Section 339.
(38) Stockmayer, W. H.; Burchard, W. *J. Chem. Phys.* **1979**, *70*, 3138.
(39) Moro, K.; Pecora, R. *J. Chem. Phys.* **1978**, *69*, 3254.

Investigation of Chain Folding in Polyethylene Melts by Diffuse Neutron Scattering†

J. Schelten* and M. Stamm

Institut für Festkörperforschung der Kernforschungsanlage Jülich, D 5170 Jülich, West Germany. *Received June 16, 1980*

ABSTRACT: Melts of polyethylene and *n*-hexatriacontane consisting of 50% deuterated and 50% protonated molecules were investigated by neutron scattering in a Q range between 0.09 and 3.25 Å^{-1}. A comparison of the measured scattering patterns with calculated scattering functions based on Gaussian chains in the melt yields no evidence for back-folding in polyethylene as proposed by Pechold. Deviations of the scattering function from the Debye function are observed. They are explained by effective intramolecular monomer–monomer interactions at the Θ temperature and are estimated from calculations based on molecular conformations obtained by Monte Carlo methods.

Introduction

There are essentially two models for the conformation of polymer molecules in the melt which are still under discussion. According to the random coil model proposed by Flory,[1] the molecular conformations in the melt and in a Θ solvent are identical, and to a first approximation the spatial distribution of two chain segments is Gaussian at large distances. For this distribution Debye developed an analytical expression for the scattering function.[2] The scattering function of single chains can be obtained by neutron scattering. With remarkable consistency it has been shown for PMMA, PS, PE, PP, and *n*-alkanes that the radii of gyration deduced from neutron small-angle scattering experiments in the melt are of the same magnitude as in Θ solvents.[3-7] In addition, the measured scattering functions in the glassy state and the melt can well be described by the Debye function within a certain Q range. Deviations from the Debye function are expected for polymers such as PE and PS for large Q values, e.g., $Q \geq 0.4$ Å^{-1}, due to influences of molecular geometry.[8] Experimentally, a Debye behavior is observed for $Q \leq 0.4$ Å^{-1}. For PMMA, on the other hand, strong deviations at much smaller Q values have been observed. By numerical calculations of scattering functions of PMMA based on the isomeric state theory it was shown that the deviations are caused by the molecular geometry.[9] Thus the experimental results from neutron scattering on polymers in the melt and in the glassy state give strong evidence that the random coil model is a good description of the polymer conformation in the melt and glassy state.

A very convincing argument for the random coil model is presented by de Gennes.[18] Intrachain and interchain forces are acting on each polymer segment. Because of the homogeneous density in amorphous polymers, the sum of both forces is independent of the molecular conformations. Therefore, the molecules coil unperturbedly and the distances between chain segments are Gaussian distributed, apart from molecular geometry effects. Despite the independence of the total segment interactions on the molecular conformation, there may exist a nonzero effective intrachain interaction, as will be discussed in the last part of the paper.

Besides this random coil model, which denies any order in the amorphous or molten state of polymers, folding models have also been proposed, e.g., the meander model of Pechold.[10,11] The essential feature of this folding model is the formation of bundles of parallel chain segments. To obtain orientational isotropy a superfolding was introduced, leading to a meander shape of the bundles. With the aid of this model it is easy to understand that polymers can crystallize rapidly since long-range diffusive motions are not necessary and that during crystallization the density changes only slightly, e.g., 14% in the case of polyethylene. Similar density differences are found for nonpolymeric organic solids. According to the random coil model, larger density differences are expected for polymers if no tendency for parallel packing of polymer segments is introduced.

In order to describe the neutron scattering experiments with polymer melts[3-8] by the meander model, a certain amount of back-folding had to be incorporated into the model (see Figure 1). The probability for back-folding is given by the Boltzmann factor $\exp(-E_f/k_BT)$. The folding energy E_f has recently been calculated on the basis of empirical interatomic potentials and a back-folding probability was obtained with which the neutron results could be explained.[12] This model is based theoretically on a few hypotheses, of which one, the cluster entropy hypothesis, cannot be proven to be either right or wrong. Up to now experimental results do not exist which are in contradiction with this model. The purpose of this paper is to present new experimental results by which a decision between the two models can be made. The basic idea of the experiments is to measure the additional scattering due to back-folding by diffuse neutron scattering from mixtures of deuterated and protonated polyethylenes in the melt. As will be shown later, this scattering should result in a halo centered at a position corresponding to the distance between neighboring chain segments.

In the theoretical section the various contributions to the scattering cross section of a polymer mixture are calculated, with emphasis on the contribution due to

† The scattering experiments were performed at the Institute Laue Langevin (ILL), Grenoble, France.

0024-9297/81/2214-0818$01.25/0